JOURNAL OF COMPUTATIONAL PHYSICS 115, 455–469 (1994)

Old and New Results on the Two-Dimensional Poiseuille Flow

A. FORTIN AND M. JARDAK

Département de Mathématiques Appliquées, École Polytechnique, C.P. 6079, Succ. "Centre-ville," Montréal, Canada, H3C 3A7

AND

J. J. GERVAIS AND R. PIERRE

Département de Mathématiques et de Statistiques, Université Laval, Québec, Canada, G1K 7P4

Received November 17, 1993; revised June 7, 1994

This paper deals with linear and non-linear hydrodynamic stability of the two-dimensional Poiseuille flow. A new numerical approach for the study of linear stability is presented. A numerical study of the transition of the flow to chaos is also presented. Using tools from dynamical system theory, we identify and characterize the different solutions of the Navier–Stokes equations at different values of the Reynolds number. Numerical solutions are presented on the unstable branch of solutions resulting from the observed subcritical Hopf bifurcation.

1. INTRODUCTION

Simple flows are extremely useful from a numerical standpoint. They play an important role, both as test cases during the development of new algorithms and as debugging tools in the construction of new codes or the updating of old ones. Among these simple flows, the most important might very well be the two-dimensional stationary laminar flow between parallel walls known as the Poiseuille flow. The geometry and boundary conditions are extremely simple. A parabolic velocity profile and constant pressure gradient solution of the analytic problem exist, for all values of the Reynolds number Re. However simple it may be, that flow has many important properties that can be useful for the numericist and which raise a number of intriguing theoretical questions, in particular, from the stability point of view. Here again, the simplicity of the geometry allows for an almost complete analysis without the use of powerful computers. Nevertheless, there is still much more to say about this flow and this is the objective of this paper. Our intention is to make a complete investigation of this problem from both the linear and non-linear stability points of view. We will also study the transition from laminar to turbulent (chaotic) flow.

We hope to demonstrate that sophisticated numerical methodologies are required to tackle the problem in all its subtleties. Until recently, this kind of analyses has been performed with the help of spectral methods; once again, the simplicity of the geometry allowed for this choice. One of our secondary objectives is to show that such analyses can be performed accurately by finite element methods.

In fluid mechanics, the role of hydrodynamic stability, which focuses on the evolution with time of small disturbances of permanent flow, is of paramount importance due to the wide range of problems arising from engineering applications. The term stable can be defined precisely in terms of those disturbances: if they ultimately decay to zero, the flow is said to be stable, whereas if any of them remains permanently different from zero, it is unstable. The study of their evolution can follow at least two roads, depending on whether the governing Navier–Stokes equations have been linearized or not: we can conduct a linear or a non-linear stability analysis. It is well known from a mathematical standpoint that steady-state solutions to the Navier–Stokes equations exist for large values of the Reynolds number Re. It is also known that for small Re the stationary solution is unique and it is of great interest, not only in the Poiseuille case for that matter, to determine for which value of Re that basic flow loses its stability. We will denote that critical value by Re_{cr}.

For Reynolds numbers higher than Re_{cr}, a number of scenarios are possible, leading to the study of transition. Surprisingly enough, the Poiseuille flow exhibits a rather complex transition at high Reynolds numbers. Another objective of this paper is to illustrate the scenario of the transition from the laminar to the turbulent state and to propose a characterization of that transition.

An outline of the paper is as follows. In Section 2, the problem is described; linear and non-linear stability are defined and discussed. Classical simplifications leading to the famous Orr–Sommerfeld differential equation are recalled. A one-dimensional analysis is performed in Section 3. The Orr–Sommerfeld equation is solved by a Ricatti method and critical Reynolds numbers are determined for different wavelengths. The same analysis is carried out in two dimensions in Section 4. A finite element method is developed for the solution of the eigenvalue problem that gives the critical Reynolds numbers. It will be clear from the development, that the latter methodol-

581/115/2-15

0021-9991/94 $6.00

ogy can be applied to more complex flows where one-dimensional analysis is not possible. Section 5 is devoted to the nonlinear stability analysis and to the study of the transition from laminar to chaotic flow. A brief conclusion follows.

2. DESCRIPTION OF THE PROBLEM

This paper focuses on the study of the flow of an incompressible fluid confined between parallel rigid walls located at $x_2 = \pm 1$ (see Fig. 1). This problem is often referred to as the Poiseuille flow. Referring again to Fig. 1, a no-slip condition is imposed on the parallel walls Γ_1 and Γ_2, while periodicity is required on the artificial boundaries Γ_3 and Γ_4, i.e.,

$$\mathbf{u}|_{\Gamma_3} = \mathbf{u}|_{\Gamma_4}. \tag{1}$$

We also impose a flowrate Q at the inlet of the domain defined by

$$Q = \int_{\Gamma_3} \mathbf{u} \cdot \mathbf{n}\, ds, \tag{2}$$

which leads us to define the Reynolds number as

$$\mathrm{Re} = \frac{3}{4}\frac{Q}{\nu}; \tag{3}$$

here ν is the kinematic viscosity. In the paper, the value of Q will always be 0 or $\frac{4}{3}$, depending on the particular form of the problem. This leads us to solve the Navier–Stokes equations which can be written in that particular case:

$$\mathcal{P}b1 = \begin{cases} \dfrac{\partial \mathbf{u}}{\partial t} - \dfrac{1}{\mathrm{Re}} \nabla \cdot (2\gamma(\mathbf{u})) + (\mathbf{u} \cdot \nabla)\mathbf{u} + \nabla \mathbf{p} = \mathbf{0} \\ \nabla \cdot \mathbf{u} = 0 \\ \mathbf{u}(\mathbf{x}, 0) = \mathbf{u}_0(\mathbf{x}) \\ \mathbf{u}|_{\Gamma_1 \cup \Gamma_2} = 0 \\ Q = \displaystyle\int_{\Gamma_3} \mathbf{u} \cdot \mathbf{n}\, ds \\ \mathbf{u}|_{\Gamma_3} = \mathbf{u}|_{\Gamma_4}, \end{cases} \tag{4}$$

where

$$\gamma(\mathbf{u})_{ij} = \frac{1}{2}\left(\frac{\partial u_i}{\partial x_j} + \frac{\partial u_j}{\partial x_i}\right). \tag{5}$$

As usual $\mathbf{x} = (x_1, x_2)$ is the position vector of an arbitrary point in the flow domain, t is the time, $\mathbf{u}$ is the velocity, and p is the pressure. It is easy to verify that a steady state solution exists for all values of Re which is given by

$$\overline{\mathbf{U}}(\mathbf{x}) = \begin{pmatrix} 1 - x_2^2 \\ 0 \end{pmatrix}, \qquad \overline{P}(\mathbf{x}) = -\frac{1}{\mathrm{Re}} x_1. \tag{6}$$

We are interested in the stability of this solution as the Reynolds number increases. Physically this can be interpreted as whether or not the steady-state solution can be observed. The basic idea is that a solution can be observed only if it is not sensitive to small perturbations. We thus suppose that at some initial moment, a small perturbation $(\mathbf{v}_0, q_0)$ is superposed to the laminar solution (6). This induces a perturbation $(\mathbf{v}, q)$ for all time $t > 0$. Stability deals with the evolution of $(\mathbf{v}, q)$ with time. It is thus necessary to obtain a set of equations describing this evolution.

Replacing $(\mathbf{u}, p)$ by $(\overline{\mathbf{U}} + \mathbf{v}, \overline{P} + q)$ in the Navier–Stokes system ($\mathcal{P}b1$) and using the fact that $(\overline{\mathbf{U}}, \overline{P})$ is a steady-state solution, we obtain the initial-value problem:

$$\mathcal{P}b2 = \begin{cases} \dfrac{\partial \mathbf{v}}{\partial t} - \dfrac{1}{\mathrm{Re}} \nabla \cdot (2\gamma(\mathbf{v})) + (\mathbf{v} \cdot \nabla)\overline{\mathbf{U}} + (\overline{\mathbf{U}} \cdot \nabla)\mathbf{v} \\ \qquad + (\mathbf{v} \cdot \nabla)\mathbf{v} + \nabla q = \mathbf{0} \\ \nabla \cdot \mathbf{v} = 0 \\ \mathbf{v}(\mathbf{x}, 0) = \mathbf{u}_0(\mathbf{x}) - \overline{\mathbf{U}} = \mathbf{v}_0(\mathbf{x}) \\ \mathbf{v}|_{\Gamma_1 \cup \Gamma_2} = 0 \\ \displaystyle\int_{\Gamma_3} \mathbf{v} \cdot \mathbf{n}\, ds = 0 \\ \mathbf{v}|_{\Gamma_3} = \mathbf{v}|_{\Gamma_4}. \end{cases} \tag{7}$$

Problem $\mathcal{P}b2$ represents the mathematical problem of hydrodynamic stability.

2.1. *Linear Stability*

Linear stability deals only with disturbances of a particular type, the form of which is suggested by experiments. In this section, we follow the approach of Georgescu [14] to get to the Orr–Sommerfeld equation. Neglecting the nonlinear term in (7) the mathematical problem of linear hydrodynamic stability becomes

$$\mathcal{P}b3 = \begin{cases} \dfrac{\partial \mathbf{v}}{\partial t} - \dfrac{1}{\mathrm{Re}} \nabla \cdot (2\gamma(\mathbf{v})) + (\mathbf{v} \cdot \nabla)\overline{\mathbf{U}} \\ \qquad + (\overline{\mathbf{U}} \cdot \nabla)\mathbf{v} + \nabla q = 0 \\ \nabla \cdot \mathbf{v} = 0 \\ \mathbf{v}(\mathbf{x}, 0) = \mathbf{v}_0(\mathbf{x}) \\ \mathbf{v}|_{\Gamma_1 \cup \Gamma_2} = 0 \\ \displaystyle\int_{\Gamma_3} \mathbf{v} \cdot \mathbf{n}\, ds = 0 \\ \mathbf{v}|_{\Gamma_3} = \mathbf{v}|_{\Gamma_4}. \end{cases} \tag{8}$$

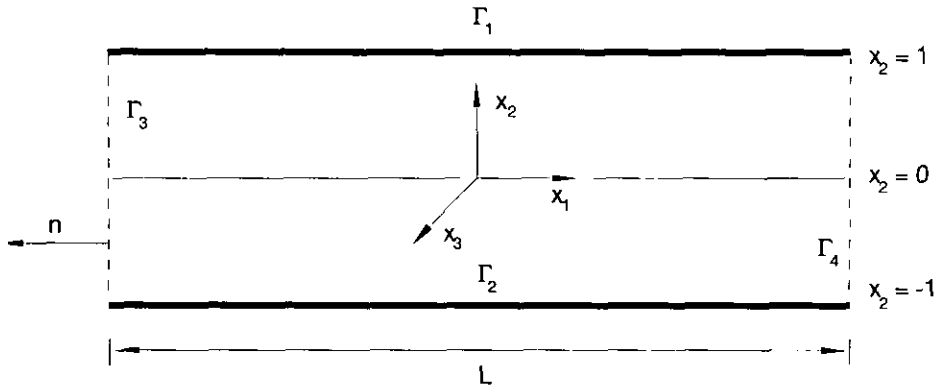

FIG. 1. Geometry of the problem.

It is assumed [1] that any perturbation $\mathbf{v}$ can be obtained by the superposition of some perturbations of the form

$$\mathbf{v}(\mathbf{x}) = \mathbf{v}_0(\mathbf{x})e^{\sigma t}, \tag{9}$$

called normal modes. In the case of unbounded domains in one direction the perturbations are assumed to be periodic along this direction. They are then of the form

$$\mathbf{v}(\mathbf{x}) = \hat{\mathbf{v}}_0(x_2)e^{i(\alpha x_1 + \sigma t)} = \hat{\mathbf{v}}_0(x_2)e^{i\alpha\left(x_1 + \frac{\sigma}{i\alpha}t\right)} \tag{10}$$

and called transversal Tollmien–Schlichting waves. Here α is the wave number in the x_1-direction ($\alpha = 2\pi/L$), L is the wavelength (length of the domain), and σ, $\mathbf{v}_0$, and q are solutions of the eigenvalue problem

$$\mathcal{P}b4 = \begin{cases} \sigma\mathbf{v}_0 + (\bar{\mathbf{U}}\cdot\nabla)\mathbf{v}_0 + (\mathbf{v}_0\cdot\nabla)\bar{\mathbf{U}} \\ \qquad -\dfrac{1}{\mathrm{Re}}\nabla\cdot(2\gamma(\mathbf{v}_0)) + \nabla q = 0 \\ \nabla\cdot\mathbf{v}_0 = 0 \\ \mathbf{v}_0|_{\Gamma_1\cup\Gamma_2} = 0 \\ \displaystyle\int_{\Gamma_3}\mathbf{v}_0\cdot\mathbf{n}\,ds = 0 \\ \mathbf{v}_0|_{\Gamma_3} = \mathbf{v}_0|_{\Gamma_4}. \end{cases} \tag{11}$$

which is obtained from $\mathcal{P}b3$ through the change of unknown (9). Let us set

$$\frac{-\sigma}{i\alpha} = c = c_r + ic_i, \tag{12}$$

so that

$$\mathbf{v}(\mathbf{x}) = \hat{\mathbf{v}}_0(x_2)e^{i\alpha(x_1 - ct)}. \tag{13}$$

For any eigenvalue and eigenfunction (σ, v_0), the corresponding wave (13) will decay to zero if and only if

$$c_i < 0. \tag{14}$$

Thus, we have linear stability if (14) is valid for all the eigenvalues and instability if it is violated by any of them. The case where the first of the c_i becomes zero is called neutral.

Since $\mathbf{v}(\mathbf{x}, t)$ is solenoidal, a stream function

$$\psi(x_1, x_2, t) = \phi(x_2)e^{i\alpha(x_1 - ct)} \tag{15}$$

can be introduced so that

$$\mathbf{v}(\mathbf{x}, t) = \begin{pmatrix} \dfrac{\partial\psi}{\partial x_2} \\ -\dfrac{\partial\psi}{\partial x_1} \end{pmatrix}. \tag{16}$$

Comparing with (13), we get

$$\hat{\mathbf{v}}_0(x_2) = \begin{pmatrix} \phi'(x_2) \\ -i\alpha\phi(x_2) \end{pmatrix}, \tag{17}$$

where the $'$ stands for the derivative with respect to x_2. Setting $q(\mathbf{x}, t) = p(x_2)e^{i\alpha(x_1 - ct)}$, the eigenvalue problem $\mathcal{P}b4$ becomes

$$\begin{aligned} &-i\alpha\phi\bar{U}_1' - i\alpha c\phi' + i\bar{U}_1\alpha\phi' = -i\alpha p + \frac{1}{\mathrm{Re}}(-\alpha^2\phi' + \phi'''), \\ &-\alpha^2 c\phi + \alpha^2\bar{U}_1\phi = -p' + \frac{1}{\mathrm{Re}}(i\alpha^3\phi - i\alpha\phi''). \end{aligned} \tag{18}$$

Upon elimination of the pressure, we obtain the well-known Orr–Sommerfeld equation

$$\begin{aligned} &(\bar{U}_1 - c)(\phi'' - \alpha^2\phi) - \phi\bar{U}_1'' \\ &\qquad = \frac{1}{i\alpha\,\mathrm{Re}}(\phi^{\mathrm{iv}} - 2\alpha^2\phi'' + \alpha^4\phi), \end{aligned} \tag{19}$$

where $\bar{U}_1 = 1 - x_2^2$ and the boundary conditions are

$$\phi(-1) = \phi'(-1) = \phi(1) = \phi'(1) = 0. \tag{20}$$

Therefore, the linear stability analysis of the sensitivity of the Poiseuille flow to perturbations of the form of transversal Tollmien–Schlichting waves is equivalent to the eigenvalue problem (19), (20), where c is the eigenvalue and ϕ is the eigenfunction.

2.2. *Non-linear Stability*

The non-linear stability analysis is based on the direct solution of $\mathcal{P}b1$ with an initial condition of the form

$$\mathbf{u}(\mathbf{x}, 0) = \bar{\mathbf{U}} + \mathbf{v}_0(\mathbf{x}), \tag{21}$$

where $\bar{\mathbf{U}}$ is again the basic flow and $\mathbf{v}_0(\mathbf{x})$ is a perturbation. The reader will easily convince himself that the resulting problem can also be obtained from $\mathcal{P}b2$ by setting $\mathbf{u} = \bar{\mathbf{U}} + \mathbf{v}$. This leads to a system that differs from $\mathcal{P}b3$ only by the inertial term $\mathbf{u} \cdot \nabla\mathbf{u}$.

3. LINEAR STABILITY: ONE-DIMENSIONAL CASE

In the preceding section, we have shown that the linear stability analysis of the Poiseuille flow, with respect to an infinitesimal two-dimensional disturbance, is equivalent to the Orr–Sommerfeld eigenvalue problem

$$(\bar{U}_1 - c)(\phi'' - \alpha^2\phi) - \phi\bar{U}_1'' = \frac{1}{i\alpha\,\mathrm{Re}}(\phi^{\mathrm{iv}} - 2\alpha^2\phi'' + \alpha^4\phi) \tag{22}$$

$$\phi(-1) = \phi'(-1) = \phi(1) = \phi'(1) = 0. \tag{23}$$

The first attempt to obtain a numerical solution of (22), (23) is due to Thomas [3]. He successfully used a finite differences scheme to tackle the numerical difficulty arising from the sharp boundary layer near the channel walls. Orszag [7] solved this problem by using an expansion in Chebyshev polynomials, and obtained $\mathrm{Re}_{cr} = 5772.22$ for $\alpha = 1.020545$. This is the smallest Reynolds number for which linear instability occurs. By varying the value of α, one can obtain the classical linear stability curve (see [1]).

We have also solved the Orr–Sommerfeld equation in order to determine critical Reynolds numbers and the corresponding eigenfunctions ϕ which will be useful for the construction of initial solutions for the two-dimensional case of the following section. For this purpose, we have chosen the Riccati method which has been introduced first by Scott [2] and subsequently applied to the Orr–Sommerfeld equation by Davey [6], Sloan [4], and Sloan and Wilks [5].

The basic idea is very simple and consists in first transforming (22) into a system of four ordinary differential equations with initial conditions. Indeed, upon rewriting (22) in the form

$$(\bar{U}_1 - c)(\phi'' - \alpha^2\phi) - \phi\bar{U}_1'' = \frac{1}{i\alpha\,\mathrm{Re}}((\phi''' - \alpha^2\phi')' - \alpha^2(\phi'' - \alpha^2\phi)) \tag{24}$$

we are led to introduce the new variables

$$\Phi = \begin{pmatrix} \phi' \\ \phi''' - \alpha^2\phi' \end{pmatrix}, \quad \Psi = \begin{pmatrix} \phi \\ \phi'' - \alpha^2\phi \end{pmatrix}, \tag{25}$$

and to rewrite (24) in the form

$$\begin{aligned} \Phi' &= \mathcal{B}\Psi \\ \Psi' &= \Phi, \end{aligned} \tag{26}$$

where $\mathcal{B}$ is the 2×2 matrix

$$\mathcal{B} = \begin{pmatrix} \alpha^2 & 1 \\ -i\alpha\,\mathrm{Re}\,\bar{U}_1'' & \alpha^2 + i\alpha\,\mathrm{Re}(\bar{U}_1 - c) \end{pmatrix}.$$

According to [1], the symmetric modes are the most destabilizing. Thus, assuming ϕ to be even, we can solve (26) on the interval $[0, 1]$ with the boundary conditions

$$\phi'(0) = \phi'''(0) = 0, \quad \phi(1) = \phi'(1) = 0. \tag{27}$$

Now, let $\mathcal{R}$ be a 2×2 matrix of the form

$$\mathcal{R} = \begin{pmatrix} r_1(x_2) & r_2(x_2) \\ r_3(x_2) & r_4(x_2) \end{pmatrix}.$$

We will say that $\mathcal{R}$ is a Riccati matrix corresponding to a solution (c, ϕ) of the eigenvalue problem (26)–(27) (or equivalently (22)–(23)) if ϕ satisfies the relation

$$\Phi = \mathcal{R}\Psi. \tag{28}$$

Since

$$\Phi(0) = \begin{pmatrix} \phi'(0) \\ \phi'''(0) - \alpha^2\phi'(0) \end{pmatrix} = \begin{pmatrix} 0 \\ 0 \end{pmatrix},$$

$$\Psi(0) = \begin{pmatrix} \phi(0) \\ \phi''(0) - \alpha^2\phi(0) \end{pmatrix},$$

the boundary condition as $x_2 = 0$ will be satisfied if

$$\mathcal{R}(0) = 0, \tag{29}$$

or, equivalently,

$$r_1(0) = r_2(0) = r_3(0) = r_4(0) = 0. \tag{30}$$

Similarly, differentiating (28) on each side, it is easily seen that (c, ϕ) is a solution of (26), if and only if $\mathcal{R}$ satisfies a system of non-linear differential equations of the form

$$\mathcal{R}' + \mathcal{R}^2 = \mathcal{B}, \tag{31}$$

which can be written as the following system of first-order ordinary differential equations:

$$\begin{aligned} r_1' &= \alpha^2 - r_1^2 - r_2 r_3 \\ r_2' &= 1 - r_1 r_2 - r_4 r_2 \\ r_3' &= 2i\alpha\,\mathrm{Re} - r_1 r_3 - r_4 r_3 \\ r_4' &= \alpha^2 + i\alpha\,\mathrm{Re}(\bar{u} - c) - r_2 r_3 - r_4^2. \end{aligned} \tag{32}$$

Looking more closely at the second and third equations, we note that they differ only by the multiplicative factor $2i\alpha$ Re. Since both r_2 and r_3 verify the same initial condition, we conclude by a unicity argument that $r_3 = 2i\alpha\,\mathrm{Re}\, r_2$. The system reduces then to three equations.

The last thing that we have to deal with is the boundary condition at $x_2 = 1$ in (27). Setting $x_2 = 1$ in (28) shows that this condition is equivalent to

$$\begin{pmatrix} 0 \\ \phi'''(1) \end{pmatrix} = \mathcal{R} \begin{pmatrix} 0 \\ \phi''(1) \end{pmatrix}$$

which, in turn, is equivalent to

$$r_2(1) = 0. \tag{33}$$

In order to determine c for given values of α and Re, one has to solve the system (32) with initial conditions (30) and under the constraint (33). This is achieved by using a shooting method. A fourth-order Runge–Kutta method is used to solve the systems of ordinary differential equations. A secant method is then used to vary the value of c until the constraint (33) is satisfied.

For example, for $\alpha = 1.020545$ and $\mathrm{Re} = 5772.22$ we found that

$$c = 0.26399856 + i\,0.25199 \times 10^{-5}$$

which is in good agreement with the result given by Orszag [7]. Once the value of c is known, the eigenfunction ϕ can be determined from (28), which, upon elimination of Φ, becomes

$$\Psi' = \mathcal{R}\Psi. \tag{34}$$

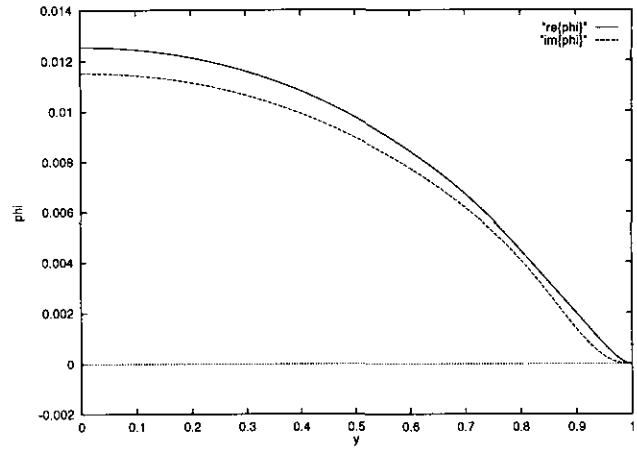

FIG. 2. ϕ.

As Ψ is not known at $x_2 = 0$ but

$$\Psi(1) = \begin{pmatrix} 0 \\ \phi''(1) \end{pmatrix},$$

a reverse integration for the solution of (34) is required. Moreover, since the solution to (34) is unique up to a multiplicative constant, we may suppose that $\phi''(1) = 1$ to get a suitable initial condition.

It is worth noting that the values of $\mathcal{R}$ which are needed to solve (34) were stored during the solution of (32). We present in Figs. 2–3, the real and complex parts of the eigenfunction ϕ and its derivative ϕ' corresponding to $\alpha = 1.020545$ and $\mathrm{Re} = 5772.22$.

4. LINEAR STABILITY: TWO-DIMENSIONAL CASE

In this section we carry out two-dimensional numerical calculations for the eigenvalue problem $\mathcal{P}b4$ in which $\overline{\mathbf{U}}$ is given by (6) and the geometry is that of Fig. 1. The results will be

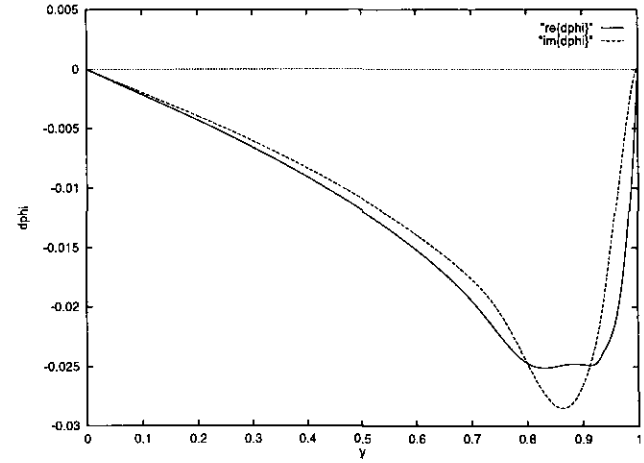

FIG. 3. ϕ'.

compared with those of the previous section. The methodology is however general and can be applied to other problems, where one-dimensional analysis is not possible (see [17] for more details).

4.1. *Our Approach*

As explained in Section 2.1, linear instability occurs when one of the c_i's becomes positive. Since $\sigma = -i\alpha c$, instability will correspond to an eigenvalue σ crossing the imaginary axis from right to left. When all eigenvalues have negative real part, the least stable mode corresponds to the σ nearest the imaginary axis.

A computation of all the eigenvalues would be prohibitive. From the above discussion, it seems plausible (but not certain) that the least stable mode can be located by looking only at the eigenvalues with smallest moduli. This can be easily done, with the help of the simultaneous inverse iteration method described in [22]. This method allows for the computation of the n_1 smallest eigenvalues in modulus of a matrix $\mathcal{A}$ of dimension N with $N \gg n_1$. The choice of n_1 is not an easy task since no indication on the position of the critical eigenvalues is available. In the following computations, n_1 was set arbitrarily to 100 (see [13] for a complete description of the method). The algorithm can be summarized as follows:

1. Construction of a random set of m initial trial vectors $\mathbf{u}_i$ stored as the columns of the $N \times m$ matrix $\mathcal{U}$.
2. Orthonormalisation of the columns of $\mathcal{U}$ by the modified Gram–Schmidt method.
3. Resolution of the m linear systems

$$\mathcal{A} \cdot \mathbf{v}_i = \mathbf{u}_i.$$

The m resulting vectors $\mathbf{v}_i$ are stored as the columns of the $N \times m$ matrix $\mathcal{V}$.

4. Reduction to $m \times m$ of the dimension of the problem

$$\mathcal{B} = \mathcal{U}^T \cdot \mathcal{V}.$$

5. Solution of the eigenproblem for $\mathcal{V}$ by the QR method

$$\mathcal{B} \cdot \mathcal{P} = \mathcal{P} \cdot \Lambda.$$

6. Inversion and sorting of the eigenvalues $\mathcal{B}$.
7. Computation of the new matrix $\mathcal{U}$,

$$\mathcal{U} = \mathcal{V} \cdot \mathcal{P}.$$

8. Convergence test. If it fails move back to 2.

In the above algorithm, the number of trial vectors m was set to $n_1 + 8$ to improve the convergence speed (see [30]).

To apply this algorithm we must first get some discrete version of $\mathcal{P}b4$ and then introduce the matrix $\mathcal{A}$. To be more explicit, let us introduce the following definitions:

$$M = \left\{ \mathbf{v} \in (H^1(\Omega))^n / \nabla \cdot \mathbf{v} = 0, \int_{\Gamma_3} \mathbf{v} \cdot \mathbf{n} = 0, \right.$$

$$\left. \mathbf{v}\Big|_{\Gamma_3} = \mathbf{v}\Big|_{\Gamma_4}, \text{ and } \mathbf{v}\Big|_{\Gamma_1 \cup \Gamma_2} = 0 \right\},$$

$$X = L^2_0(\Omega).$$

Clearly M is a subspace of the Sobolev space $(H^1(\Omega))^n$. Defining $\mathcal{A}$ as the $N \times N$ matrix related to the finite element discretization of the operator

$$(\bar{\mathbf{U}} \cdot \nabla)\mathbf{u} + (\mathbf{u} \cdot \nabla)\bar{\mathbf{U}} - \frac{1}{\mathrm{Re}} \nabla \cdot (2\gamma(\mathbf{u})), \tag{35}$$

defined on M, the problem $\mathcal{P}b4$ has the variational form

$$\mathcal{P}b7 = \begin{cases} \text{Find } \mathbf{v}_0 \in M \\ (\mathcal{A}\mathbf{v}_0, \mathbf{v}) = (-\sigma \mathbf{v}_0, \mathbf{v}) \quad \forall \mathbf{v} \in M. \end{cases} \tag{36}$$

where $(\cdot, \cdot)$ designate the scalar product in $L^2(\Omega)$. Problem $\mathcal{P}b4$ is an eigenvalue problem on the subspace M of divergence-free periodic functions satisfying homogeneous boundary conditions and for which the flowrate is 0 on Γ_3. Step 3 of the algorithm requires the solution of a sequence of problems of the form

$$\mathcal{P}b8 = \begin{cases} \text{For each } i = 1, 2, 3, \ldots, m, \text{ find } \mathbf{v}_i \in M \\ (\mathcal{A}\mathbf{v}_i, \mathbf{v}) = (\mathbf{u}_i, \mathbf{v}) \quad \forall \mathbf{v} \in M. \end{cases} \tag{37}$$

The problems $\mathcal{P}b8$ are constrained problems with solutions in M and, following Fortin [8, 9], they can be solved with the help of the following algorithm:

For $i = 1, 2, 3, \ldots, m$,
step 0: $\mathbf{v}_i^0, p^0, \lambda^0$ given arbitrarily

step 1: **For** $k \geq 0$, solve ($\mathbf{v}_i^k, p^k, \lambda^k$ being known)

$$\int_\Omega \left\{ \frac{2}{\mathrm{Re}} \gamma(\delta\mathbf{v}_i^k) : \gamma(\mathbf{w}) + (\bar{\mathbf{U}} \cdot \nabla)\delta\mathbf{v}_i^k \mathbf{w} \right.$$

$$\left. + (\delta\mathbf{v}_i^k \cdot \nabla)\bar{\mathbf{U}}\mathbf{w} + r_1 \nabla \cdot \delta\mathbf{v}_i^k \nabla \cdot \mathbf{w} \right\} dx$$

$$+ r_2 \left(\int_{\Gamma_3} \delta\mathbf{v}_i^k \cdot \mathbf{n}\, ds \right) \left(\int_{\Gamma_3} \mathbf{w} \cdot \mathbf{n}\, ds \right) =$$

$$\int_\Omega \left\{ \frac{2}{\mathrm{Re}} \gamma(\mathbf{v}_i^k) : \gamma(\mathbf{w}) + (\bar{\mathbf{U}} \cdot \nabla)\mathbf{v}_i^k \mathbf{w} \right.$$

$$\left. + (\mathbf{v}_i^k \cdot \nabla)\bar{\mathbf{U}}\mathbf{w} - \mathbf{u}_i \mathbf{w} - p^k \nabla \cdot \mathbf{w} \right\} dx$$

$$+ \lambda^k \left(\int_{\Gamma_3} \mathbf{w} \cdot \mathbf{n}\, ds \right)$$

Step 2: Update

$$\mathbf{v}_i^{k+1} = \mathbf{v}_i^k - \delta\mathbf{v}_i^k$$

$$p^{k+1} = p^k - r_1 \nabla \cdot \mathbf{v}_i^k$$

$$\lambda^{k+1} = \lambda^k - r_2 \left(\int_{\Gamma_3} \mathbf{v}_i^k \cdot \mathbf{n}\, ds \right).$$

This algorithm is based on a generalization of the Uzawa algorithm for the solution of saddle-point problems [12]. The constraints

$$\nabla \cdot \mathbf{v}_i = 0, \quad \int_{\Gamma_3} \mathbf{v}_i \cdot \mathbf{n}\, ds = 0,$$

are both imposed through the Lagrange multipliers p and λ, respectively. Moreover, the constraints are strongly penalized, with penalization parameters r_1 and r_2 of the order of 10^7. As mentioned in [9], the velocities and pressure cannot be chosen independently. The $\mathbf{Q}_2 - \mathbf{P}_1$ (Fig. 4) element was used for the discretization of the velocity components and pressure since it is well known that this is one of the best elements for two-dimensional simulations. In fact this element is second order in space ($O(h^2)$) and satisfies the **inf-sup** condition of Brezzi [15] by passing the test of Fortin [11].

The choice of the mesh is another important issue. We have used four different meshes depicted in Figs. 5–8. On each of these meshes, the eigenvalues were computed for $\alpha = 1.020545$ and Re = 5772.22. The following values (Table I) were obtained for the smallest eigenvalue crossing the imaginary axis.

The value of c on mesh 4 agrees to six digits for the one-dimensional computation with the Orr–Sommerfeld equation. This mesh will be used in all subsequent computations. If one determines critical Reynolds numbers corresponding to various α by finding the first value of Re for which one (or more) eigenvalues crosses the imaginary axis, one gets a curve as in Fig. 9 which is called a neutral stability curve. One can also fix α and study the variation of the eigenvalues with Re. This is illustrated in Figs. 10–13, which show that, as Re increases, a pair of conjugate eigenvalues crosses the imaginary axis. For $\alpha = 1.020545$ this occurs at Re $\simeq$ 5772.22.

4.2. *Ghaddar's Approach*

Another approach to the study of linear stability was described by Ghaddar, Korczak, Mikic, and Patera [16]. Rather

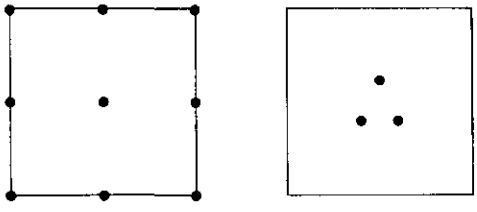

FIG. 4. Element $\mathbf{Q}_2 - \mathbf{P}_1$.

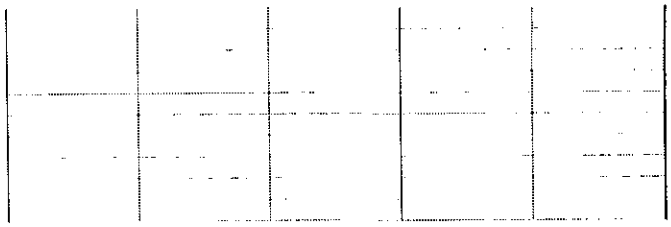

FIG. 5. Mesh 1.

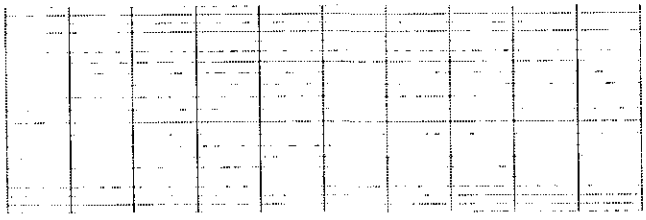

FIG. 6. Mesh 2.

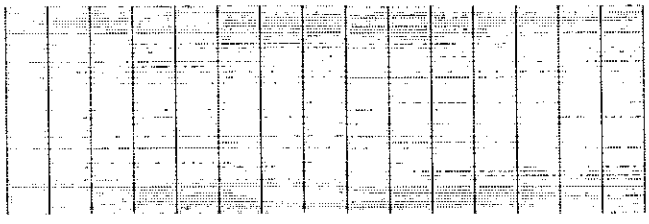

FIG. 7. Mesh 3.

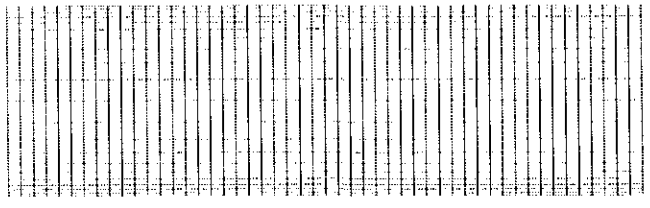

FIG. 8. Mesh 4.

TABLE I

Mesh	σ	$c = -\sigma/i\alpha$
1	$0.21689 \times 10^{-1} \pm 0.31649i$	$0.31011861 \pm 0.2125237i \times 10^{-1}$
2	$0.90832 \times 10^{-3} \pm 0.27084i$	$0.26538761 \pm 0.8900342i \times 10^{-3}$
3	$-0.33565 \times 10^{-4} \pm 0.26946i$	$0.26403539 \pm 0.3288929i \times 10^{-4}$
4	$-0.73643 \times 10^{-5} \pm 0.26944i$	$0.26401581 \pm 0.7216046i \times 10^{-5}$

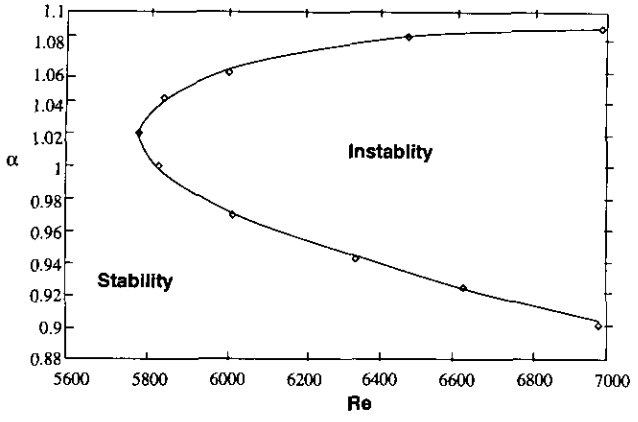

FIG. 9. Neutral stability curve.

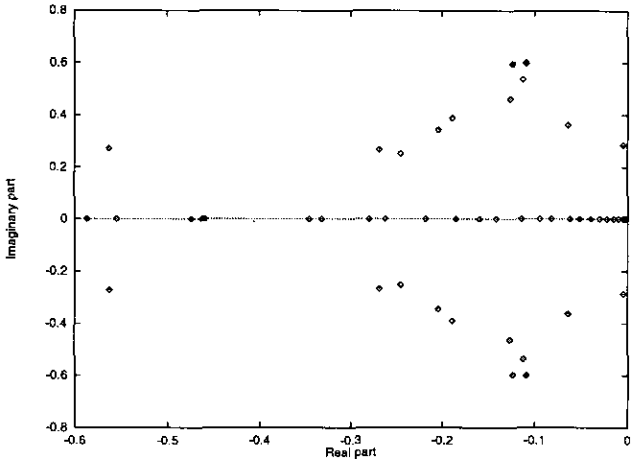

FIG. 10. Eigenvalues for Re = 4000 and $\alpha = 1.020545$.

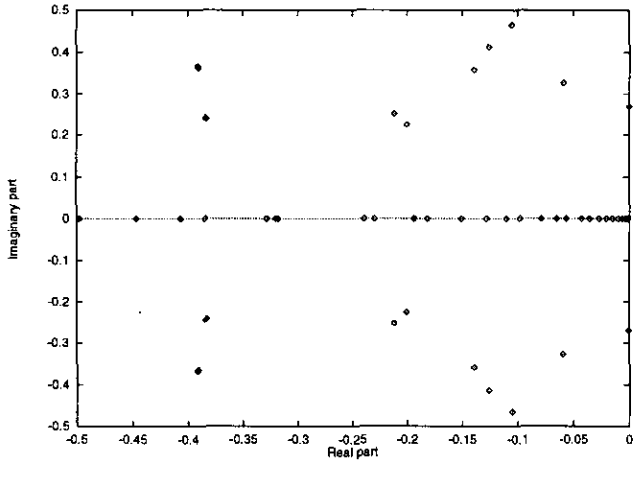

FIG. 11. Eigenvalues for Re = 5772.22 and $\alpha = 1.020545$.

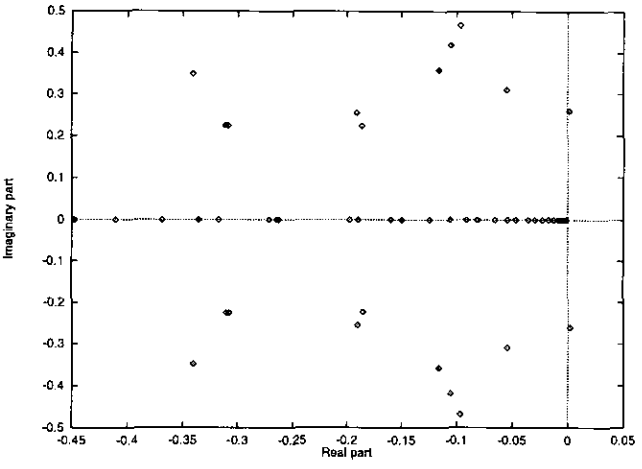

FIG. 12. Eigenvalues for Re = 7000 and $\alpha = 1.020545$.

than looking at perturbations of the specific type (10), they propose to solve $\mathcal{P}b3$ directly with the initial condition

$$\mathbf{v}(\mathbf{x}, 0) = \Re e(\hat{\mathbf{v}}_0(x_2)e^{i\alpha x_1}); \tag{38}$$

i.e., the real part of the transversal Tollmien–Schlichting wave at $t = 0$. $\hat{\mathbf{v}}_0(x_2)$ is the least stable mode obtained from the resolution of the Orr–Sommerfeld equation and by the relation (17). Using the numerical solution of the velocity at a representative point in the domain, they read off the growth rate $\tilde{\sigma}$ and the frequency $\tilde{\Omega}$. We followed their approach and resolved, in turn, the same problem, using our finite element code. For the time discretization, we used a fully implicit Gear scheme defined by

$$\frac{\partial \mathbf{u}}{\partial t} = \frac{3\mathbf{u}^{n+1} - 4\mathbf{u}^n + \mathbf{u}^{n-1}}{2\,\Delta t}. \tag{39}$$

At Re = 525 and for $\alpha = 0.94244778$, we obtained at the point (5.312743, 0.96992737) the signal depicted in Fig. 14.

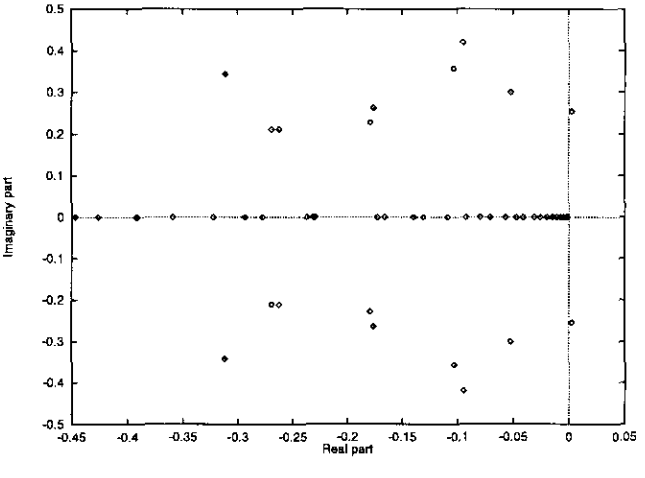

FIG. 13. Eigenvalues for Re = 8000 and $\alpha = 1.020545$.

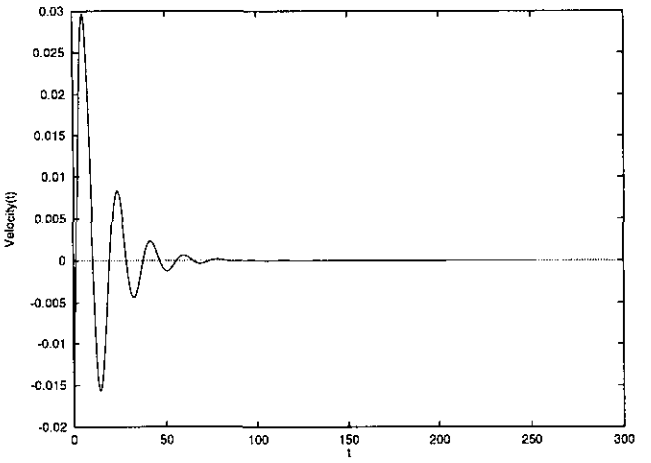

FIG. 14. Evolution of the perturbation.

By the means of a non-linear regression, we obtained $\tilde{\sigma} = -0.0699295$ as a growth rate and $T = 18.20$ as the period. The frequency is then $\tilde{\Omega} = 0.054945$, which is in good agreement with the results of Ghaddar *et al.* [16] and Orszag [7]. It is worth noting that the shape of the streamlines at $t = 0$ and $t = T$ is virtually preserved as shown in Figs. 15–16, an indication of the accuracy of our numerical scheme. To verify the above results, we have computed the eigenvalues using the approach of Section 4.1. We have obtained

$$\sigma = -0.06996 \pm i\, 0.34541,$$

for the least stable mode. A simple calculation gives a frequency of

$$\tilde{\Omega} = 0.0549737,$$

which agrees with the result of Ghaddar. The encircled dots of Fig. 17 represent this pair of eigenvalues.

5. TRANSITION

The objective of this section is to understand how, and under what circumstances, transition from steady to chaotic flow occurs, in the case of Poiseuille flow. Such transition cannot be predicted by linear theory. Consequently, the full two-dimensional Navier–Stokes equations will be solved starting at Reynolds numbers where linear stability is lost. For $\alpha = 1.020545$ this occurs at Re = 5772.22. The Reynolds number is then slowly increased and the different solutions are analysed by means of Fourier analysis and phase portraits. This allows the identification of the bifurcations occurring in the flow problem. One goal of the numerical experiments carried out in this section

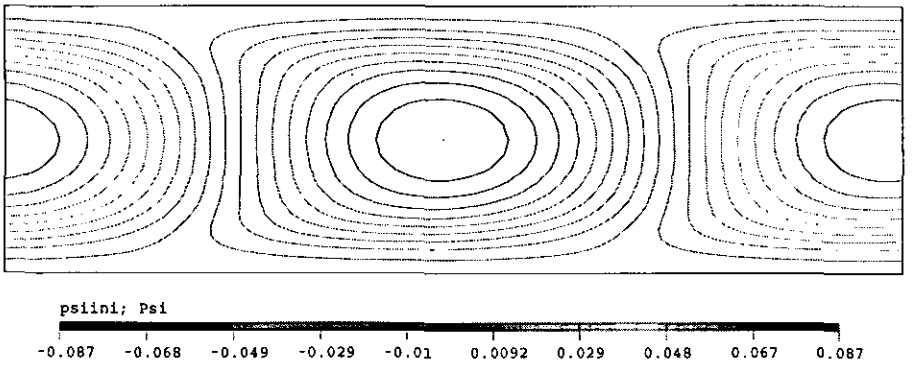

FIG. 15. Streamlines at $t = 0$.

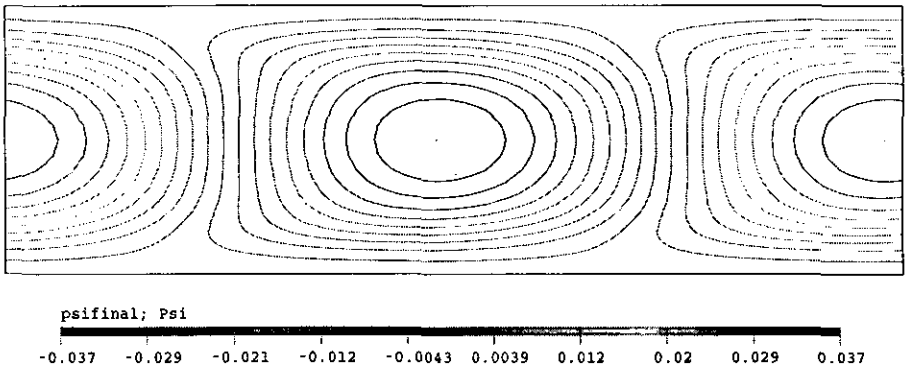

FIG. 16. Streamlines at $t = T$.

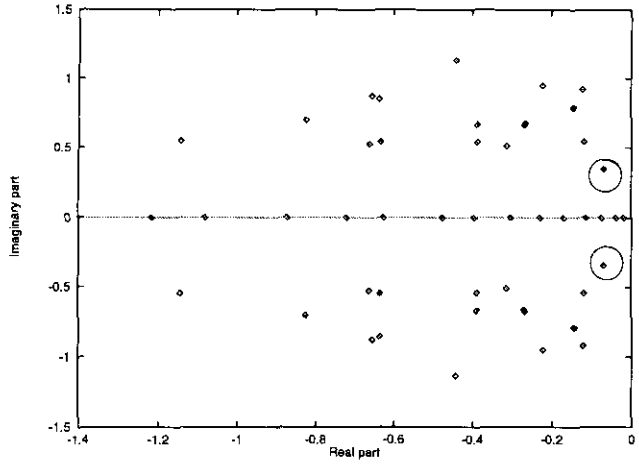

FIG. 17. Eigenvalues for Re = 525 and $\alpha = 0.9424778$.

is to establish, if possible, a link with fundamental theoretical works.

5.1. *Numerical Method*

The study of the transition and of the non-linear stability of the steady flow can be done by examination of the behavior of the solution of the problem $\mathcal{P}b1$ with the particular initial condition

$$\mathbf{u}(\mathbf{x}, 0) = \overline{U} + \mathbf{v}_0(\mathbf{x}). \tag{40}$$

The initial perturbation $\mathbf{v}_0$ is given here again by (38). Problem $\mathcal{P}b1$ is then solved by using a slight modification of the algorithm of Section 4, since in this case the flowrate Q is different from 0. A fully implicit Gear scheme (39) was used for the discretization of the time derivative. This difference equation is second-order accurate $O(\Delta t^2)$ and is known to be A stable.

5.2. *Numerical Results*

The first numerical results presented in this section were computed for $\alpha = 1.020545$ using mesh 4 of Fig. 8 for which the computation of the eigenvalues of the problem $\mathcal{P}b6$ was the most accurate. Other values of α will be considered later.

Since snapshots of streamlines and of the velocity field are not sufficient to get a complete picture of the solutions at different Reynolds numbers, we introduce two tools from dynamical systems theory: phase portraits and Fourier analysis. For more details about the construction of phase portraits and the Fourier analysis, the reader is referred to [10]. These tools allow us to characterize and classify solutions and also to localize the values of the Reynolds numbers where bifurcations occur.

The following strategy was used. At each time step the values of the velocity field at three points in the domain represented in Fig. 1 were stored. The time step Δt was set to 0.05 during all computations, and at least 100,000 time-steps were required to obtain a solution for each Reynolds number. Phase portraits were then constructed and a Fourier analysis was performed using the resulting signal.

At low Reynolds numbers, the steady flow is stable and the parabolic profile (6) is recovered as predicted by the linear theory and as can be seen in Fig. 18. The oscillations introduced by the perturbation decays until the velocity profile becomes parabolic again. At Re $\simeq$ 5772.22, according to the results of Sections 3 and 4, a pair of conjugate eigenvalues crosses the imaginary axis leading the flow to become unstable. This is an indication of a Hopf bifurcation. It is known [24] that this bifurcation is subcritical. Consequently, the branch of periodic solutions bifurcates in the direction of decreasing Reynolds numbers and the bifurcating solutions are unstable. Figure 19 gives the expected bifurcation diagram. In order to get on the upper branch at point A, we solved the problem at Re = 5772.22 and we obtained a periodic flow with a non-vanishing amplitude that depends on Re and on the wave number α. The fundamental frequency f_1 is essentially the same as the one found in the previous section. In Fig. 20 we can see the meandering of the central flow. The temporal evolution of the velocity, the phase diagram, and the Fourier analysis are presented respectively in Figs. 21, 22, and 23. As expected, the velocity at a given point in the domain is perfectly periodic. This is confirmed by the Fourier analysis showing a fundamental frequency and a few harmonics and by the closed curve of the phase portrait.

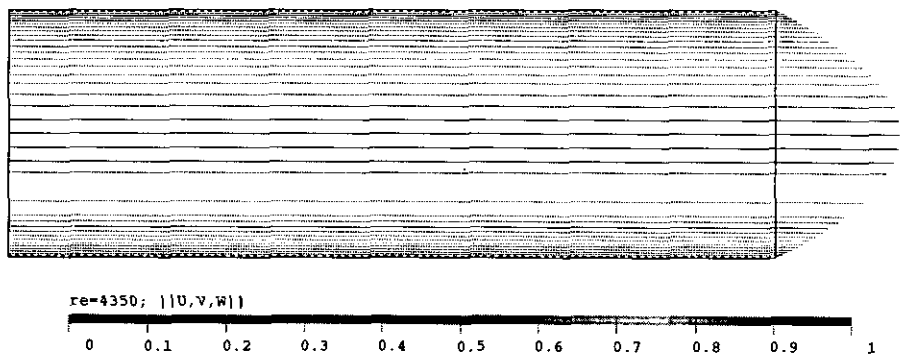

FIG. 18. Laminar flow velocity.

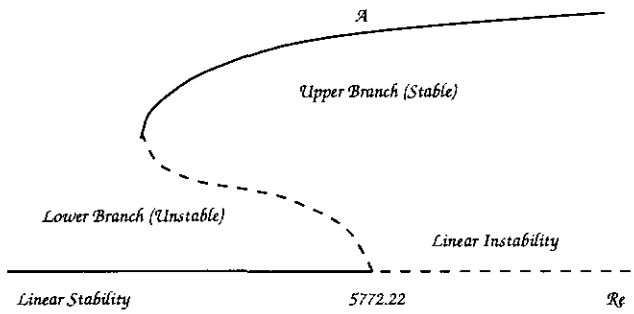

FIG. 19. Sketch of the bifurcation diagram.

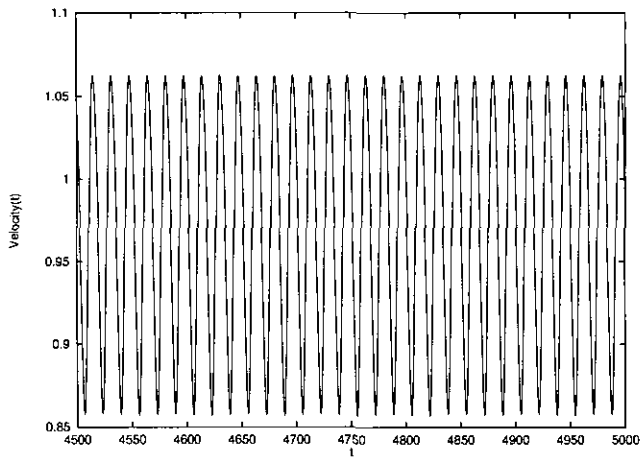

FIG. 21. Time evolution for Re = 5772.22.

As the Reynolds number is increased, this time-periodic solution remains stable up to Re = 6000, where a second incommensurate frequency f_2 appears. The velocity field is presented in Fig. 24 and it is easily seen in Fig. 25 that the signal is quasi-periodic. This is confirmed by the phase portraits that are now projections in the plane of a two-dimensional torus as shown in Fig. 26. Figure 27 is the Fourier analysis of the signal showing the presence of a second frequency of very small amplitude.

For Re = 8000 and Re = 10,000 the flow is still quasi-periodic, although the meandering of the central flow is more pronounced. At the bends in the flow, cat's-eye patterns can be observed (see Fig. 28) as described in [28, 20]. The second frequency has increased in amplitude as can be seen in Fig. 29.

At Re $\simeq$ 11,000, the time evolution of the oscillations becomes weakly chaotic. This chaotic behaviour increases with the Reynolds number as shown in Figs. 30–32 for Re = 12,900. The velocity signal has no regularity at all (Fig. 31) and the Fourier analysis presented in Fig. 33 shows the emergence of a broadband component. Finally the phase portrait is no longer a torus and presents very irregular patterns (see Fig. 32).

During our numerical experiments, we did not detect the presence of frequency locking as in Jimenez [21], who did his calculations with α = 1.0. Having a two-parameter (α and Re) dependent dynamical system it is known (see, e.g., Guckenheimer and Holmes, Chap. 6 in [29]) that frequency locking is likely to occur for an open set in the (α–Re) space parameters. If one knows how to control one parameter while the other varies monotonously, the frequency locking may be observed on a relatively large range of the second parameter. If only one parameter varies, frequency locking may occur on a very small range of this parameter. This is most likely what happened since α was fixed at 1.020545. We did not manage to increase the Reynolds number very slowly in order to get frequency locking, due to a prohibitive computational cost. Consequently, we cannot confirm nor refute the results of Jimenez [21] concerning the presence of frequency locking.

In order to determine more precisely the nature of the bifurcation occurring at Re = 5772.22 and to confirm the bifurcation diagram in Fig. 19, it seemed interesting to make some more computations starting at Re = 6000 and decreasing Re gradually. In each case the initial condition was taken as the converged solution obtained at the previous Reynolds number.

We were able to obtain periodic solutions for Reynolds numbers as low as 4350. At Re $\simeq$ 4350 with α always set at 1.020545 the steady flow reappears again. This result agrees with those of Zahn [23]. In fact a close look at the so-called metastable regions of [23] shows the accuracy of our result.

To complete and validate our results, computations were performed for two other values of α. At α = 1.3126, the lowest Reynolds for which we could find a periodic solution was 2645 and at α = 1.310, we found Re $\simeq$ 2680 again in good

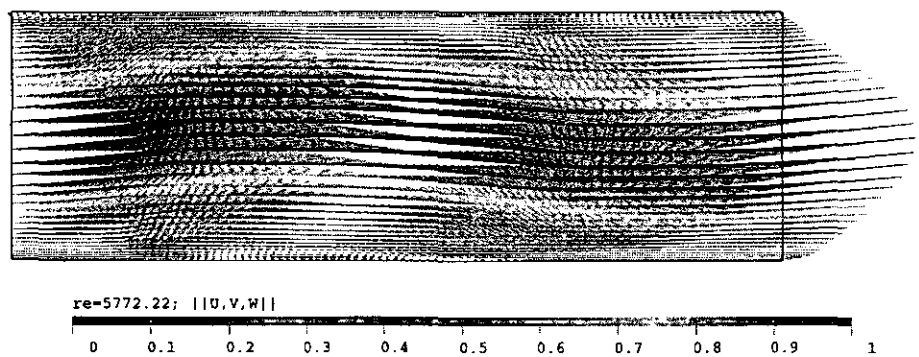

FIG. 20. Velocity field for Re = 5772.22.

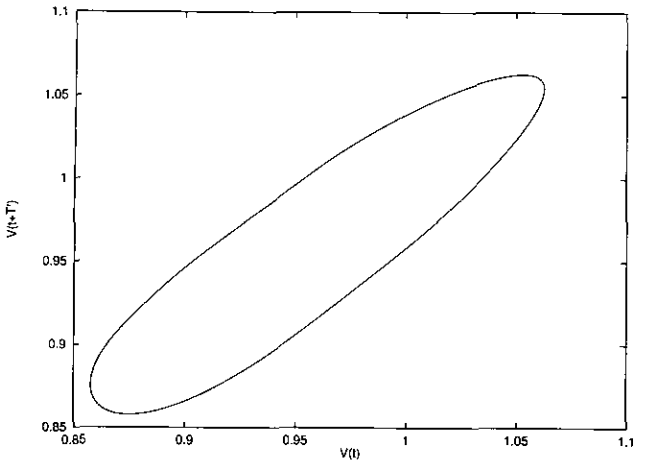

FIG. 22. Phase diagram for Re = 5772.22 ($T' = 0.25$).

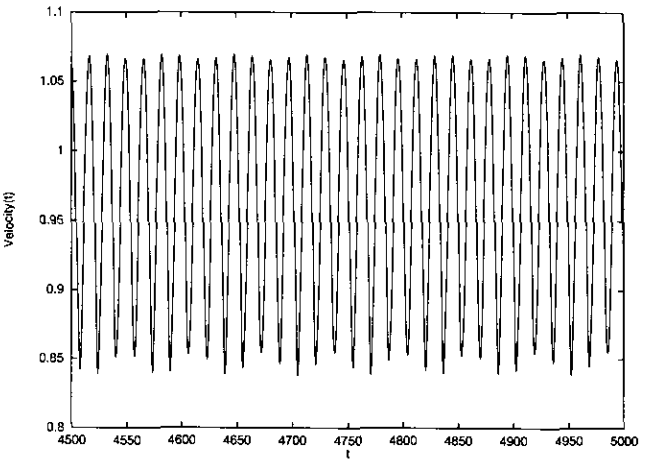

FIG. 25. Time evolution for Re = 6000.

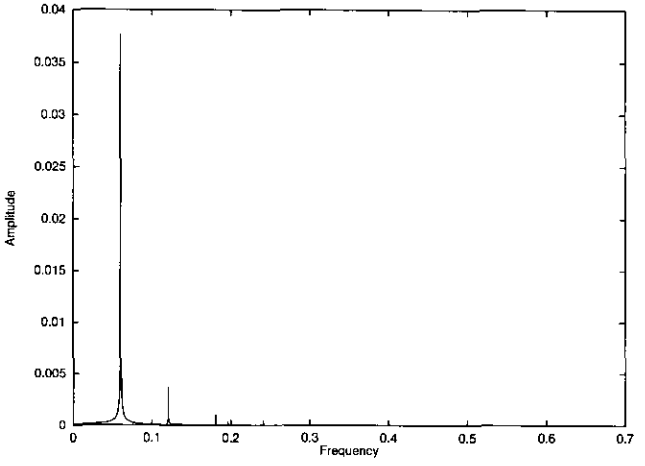

FIG. 23. Fourier analysis for Re = 5772.22.

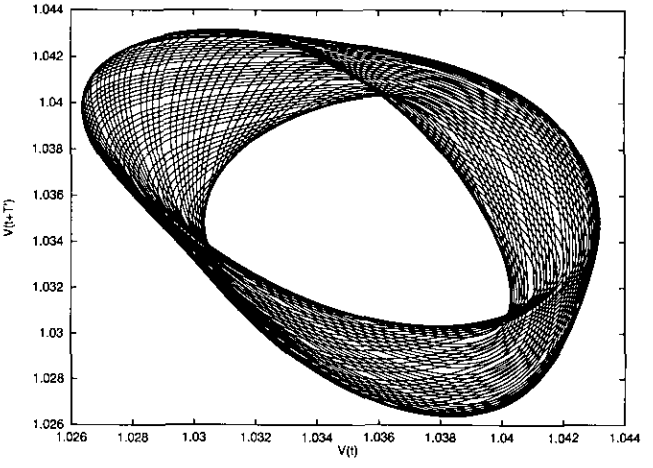

FIG. 26. Phase diagram for Re = 6000 ($T' = 0.25$).

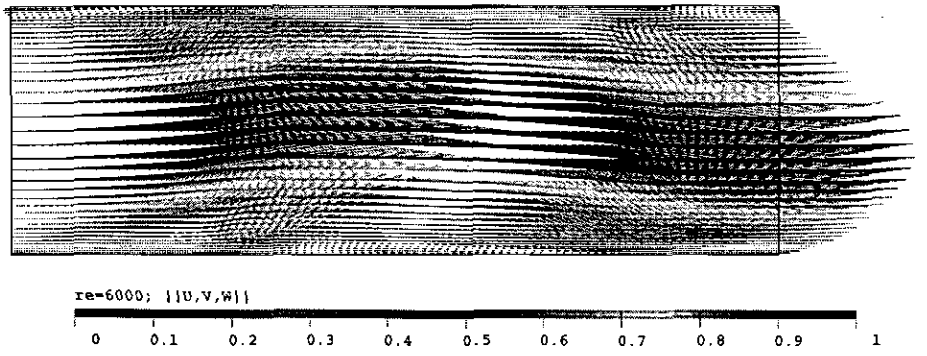

FIG. 24. Velocity field for Re = 6000.

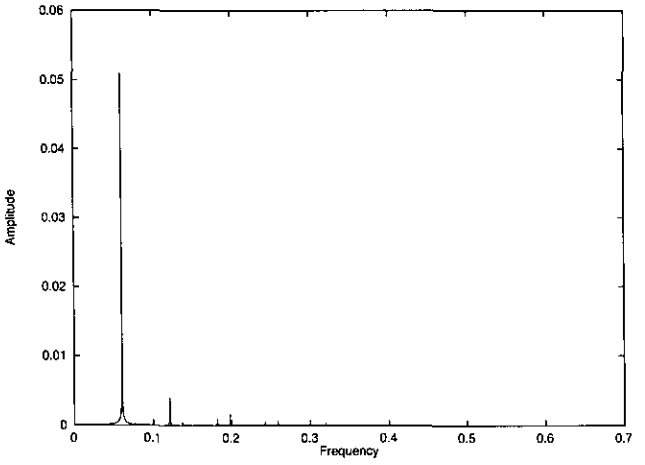

FIG. 27. Fourier analysis for Re = 6000.

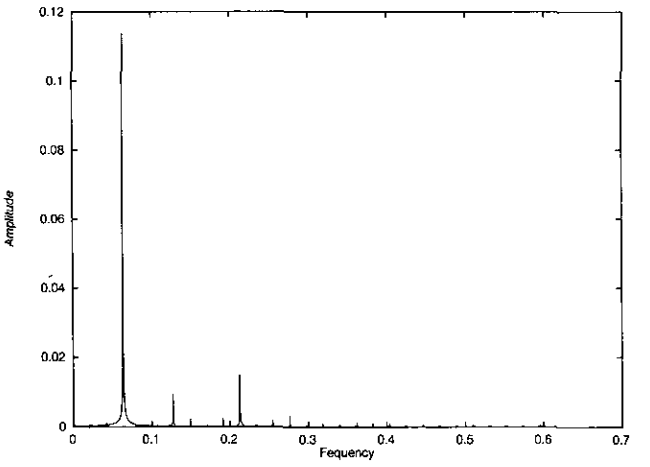

FIG. 29. Fourier analysis for Re = 10,000.

agreement with the results of Zahn [23] and also with those of Joseph [27].

Figure 34 shows the decay of the amplitude with the Reynolds number for $\alpha = 1.020545$. Figure 35 illustrates how the signal is vanishing for Re = 4350. Figure 36 gives a sketch of the amplitude versus Re for $\alpha = 1.3126$. This value of α gives the smallest Reynolds number for which a periodic solution can be observed.

From these results we deduce that the turning point of the bifurcation diagram occurs around Re $\simeq$ 2645 and the amplitude of the unstable periodic solutions on the lower branch are very small. In particular, we recover the well-known observations that the domain of attraction of the laminar solution in the subcritical range ($2645 \leq \text{Re} \leq 5772.22$, according to our computations) is very small. Consequently, in the subcritical range of Reynolds numbers, any slight perturbation of the Poiseuille flow, apart from a very small one, will lead the flow to escape the domain of attraction of the Poiseuille flow and snaps through the unstable bifurcating branch to a flow with a large amplitude, not necessarily a periodic flow belonging to the upper branch. This is the so-called snap through instability mechanism as explained in [24].

6. CONCLUSION

We have developed a practical and accurate numerical method for the study of the linear hydrodynamic stability of the two-dimensional Poiseuille flow. This method gives satisfactory results when compared to other methods. The most important feature of this method is that it can be applied to more general problems especially those where the steady solution is not known exactly as is the case with the Poiseuille flow.

We have presented the phenomenology of transition and nonlinear stability. Our results seem to confirm a few theoretical results. They are also in good agreement with experimental observations.

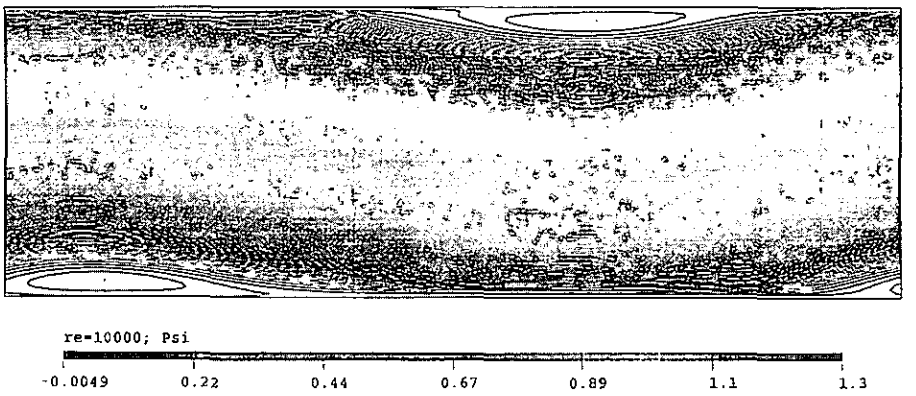

FIG. 28. Streamlines for Re = 10,000.

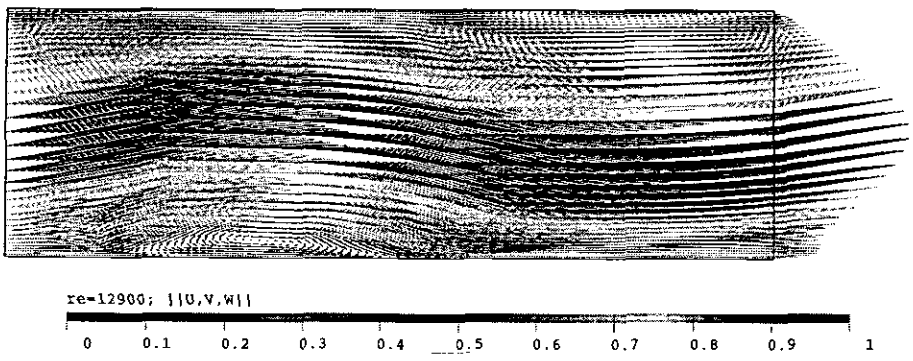

FIG. 30. Velocity field for Re = 12,900.

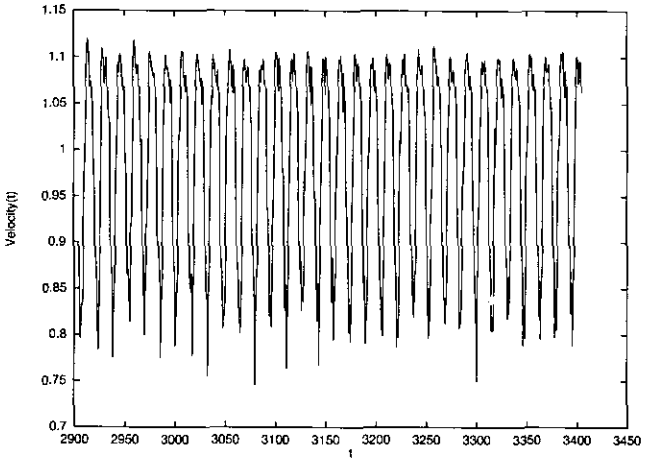

FIG. 31. Time evolution for Re = 12,900.

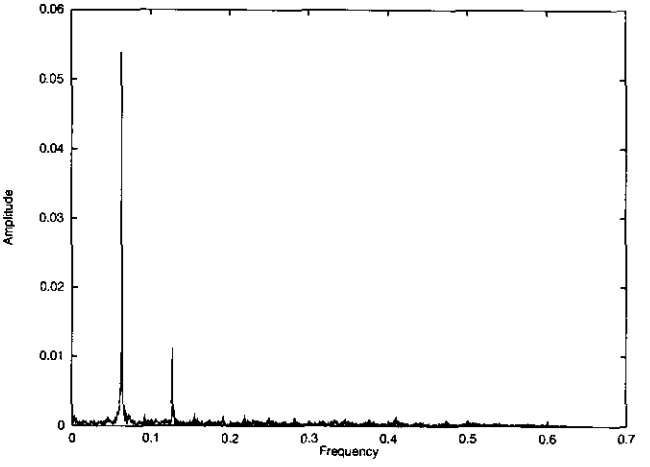

FIG. 33. Fourier analysis for Re = 12,900.

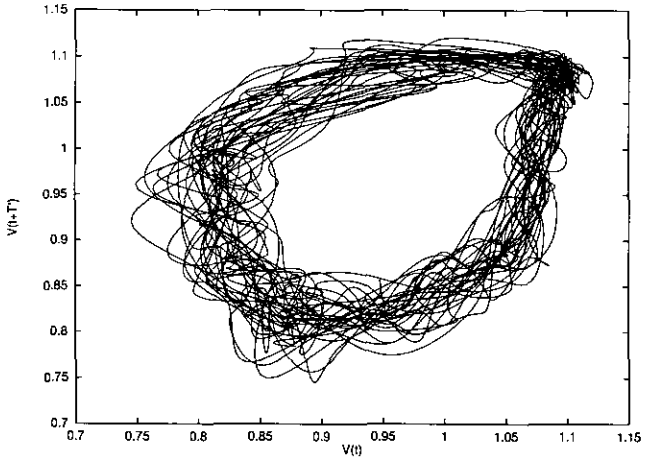

FIG. 32. Phase diagram for Re = 12,900 ($T' = 0.25$).

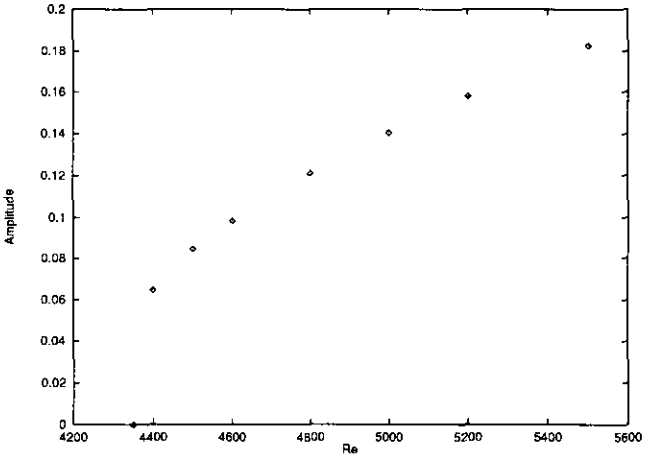

FIG. 34. Sketch of the amplitude versus Re for $\alpha = 1.020545$.

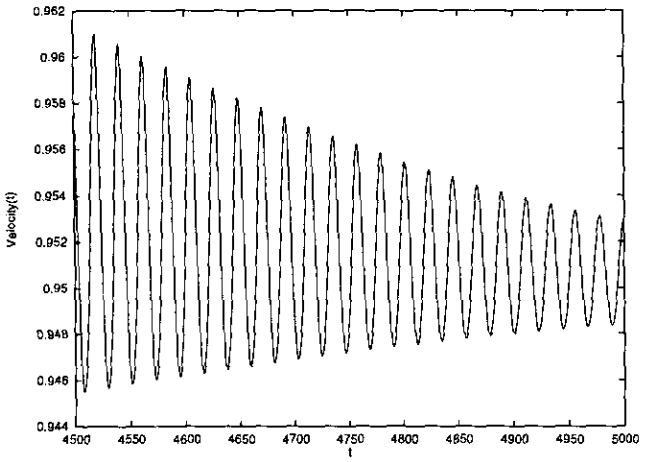

FIG. 35. Time evolution of the velocity.

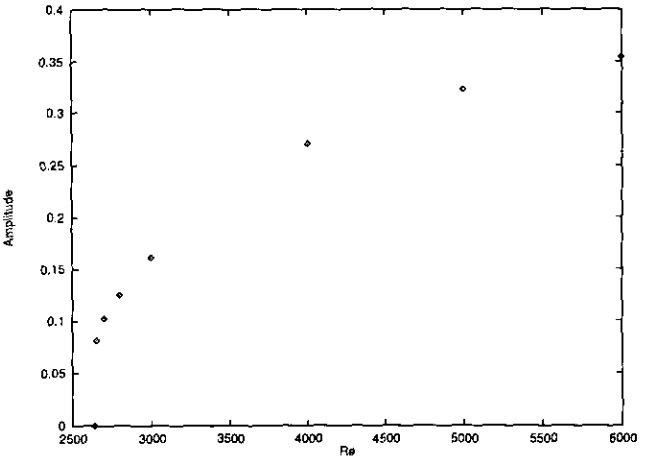

FIG. 36. Sketch of the amplitude versus Re for $\alpha = 1.3126$.

REFERENCES

1. P. G. Drazin and W. H. Reid, *Hydrodynamic Stability* (Cambridge Univ. Press, Cambridge, UK, 1981).
2. M. R. Scott, *J. Comput. Phys.* **12,** 334 (1973).
3. L. H. Thomas, *Phys. Rev.* (2), **91,** 780 (1953).
4. D. M. Sloan, *J. Comput. Phys.* **24,** 320 (1977).
5. D. M. Sloan and G. Wilks, *J. Comput. Appl. Math.* **3,** 195 (1977).
6. A. Davey, *J. Comput. Phys.* **24,** 331 (1977).
7. S. A. Orszag, *J. Fluid Mech.* **50,** 689 (1971).
8. A. Fortin, Commun. Appl. Numer. Methods **4,** 835 (1988).
9. A. Fortin, M. Fortin, and J. J. Gervais, *Theoret. Comput. Fluid Dynamics* **3,** 79 (1991).
10. A. Fortin, M. Fortin, and J. J. Gervais, *J. Comput. Phys.* **70,** 295 (1987).
11. M. Fortin, *Int. J. Numer. Methods Fluids* **1,** 347 (1981).
12. M. Fortin and A. Fortin, *Commun. Appl. Numer. Methods* **1,** 205 (1985).
13. W. J. Stewart and A. Jennings, *ACM Trans. Software* **7**(2), 184 (1981).
14. A. Georgescu, *Hydrodynamic Stability Theory* (Nijhoff, Doldrecht, 1985).
15. F. Brezzi and M. Fortin, *Mixed and Hybrid Finite Element Methods* (Springer-Verlag, New York, 1991).
16. N. K. Ghaddar, K. Z. Korczak, B. B. Mikic, and A. T. Patera, *J. Fluid. Mech.* **163,** 99 (1986).
17. A. Fortin and M. Jardak, in preparation.
18. D. Sattinger, *Topics in Stability and Bifurcation Theory,* Lecture Notes in Mathematics, Vol. 309 (Springer-Verlag, Berlin/Heidelberg/New York, 1973).
19. J. T. Stuart, *J. Fluid. Mech.* **163,** 1 (1958).
20. J. T. Stuart, *Annu. Rev. Fluid. Mech.* **3,** 347 (1971).
21. J. Jimenez, *J. Fluid. Mech.* **218,** 265 (1990).
22. M. El Hajji, Ph.D. thesis, Université Laval, Québec, 1991 (unpublished).
23. J.-P. Zahn, J. Toomre, E. A. Spiegel, and D. O. Gough, *J. Fluid. Mech.* **64**(2), 319 (1974).
24. D. D. Joseph and D. H. Sattinger, *Arch. Rat. Mech. Anal.* **45,** 79 (1972).
25. W. C. Reynolds and M. C. Potter, *J. Fluid. Mech.* **27**(3), 465 (1967).
26. C. L. Perkis and B. Shkoller, *J. Fluid. Mech.* **29**(1), 31 (1967).
27. D. D. Joseph and T. S. Chen, *J. Fluid. Mech.* **66,** 79 (1972).
28. R. F. Bergeron, *Stud. Appl. Math.* **49,** 197 (1970).
29. J. Guckenheimer and P. Holmes, *Nonlinear Oscillations, Dynamical Systems and Bifurcations of Vector Fields* (Springer-Verlag, New York, 1983).
30. K-J. Bathe and E. L. Wilson, *Numerical Methods in Finite Element Analysis* (Prentice-Hall, Englewood Cliffs, NJ, 1976).